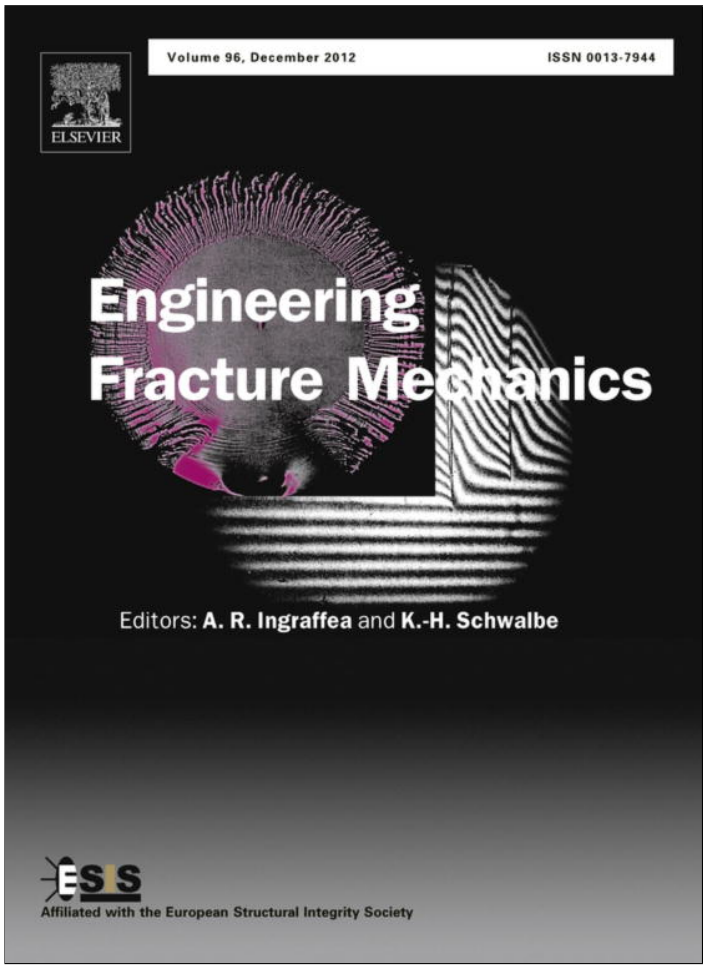

Engineering Fracture Mechanics 96 (2012) 724–736

Contents lists available at SciVerse ScienceDirect

Engineering Fracture Mechanics

journal homepage: www.elsevier.com/locate/engfracmech

# Evaluation of bone cohesive laws using an inverse method applied to the DCB test

F.A.M. Pereira [a,b], J.J.L. Morais [a], M.F.S.F. de Moura [b,*], N. Dourado [a], M.I.R. Dias [c]

[a] CITAB/UTAD, Departamento de Engenharias, Quinta de Prados, 5001-801 Vila Real, Portugal
[b] Faculdade de Engenharia da Universidade do Porto, Departamento de Engenharia Mecânica e Gestão Industrial, Rua Dr. Roberto Frias, 4200-465 Porto, Portugal
[c] UTAD, Departamento de Ciências Veterinárias, Quinta de Prados, 5001-801 Vila Real, Portugal

ARTICLE INFO

*Article history:*
Received 7 May 2012
Received in revised form 4 August 2012
Accepted 1 October 2012

*Keywords:*
Bone
Fracture characterization
Mode I
Cohesive laws

ABSTRACT

The double cantilever beam test was used to measure the mode I fracture properties of bovine cortical bone. Hydrated and dehydrated bone was used as testing material with the objective to analyze the influence of water on bone fracture toughness. Additionally, water influence on the elastic modulus and on the material brittleness was also assessed by means of the flexure and microhardness Vickers tests, respectively. Two different data reduction schemes were utilized to determine the Resistance-curve of hydrated and dehydrated bone, both allowing the measurement of bone fracture toughness. Cohesive laws describing fracture behavior were determined from measured fracture energies through an inverse method, based on a developed genetic algorithm combined with finite element simulation of the double cantilever beam test. Two different types of laws were identified owing to dissimilar fracture behavior observed for the hydrated and dehydrated young bovine bone. It was verified that water plays a fundamental role in which concerns the material ductility which reflects on completely different fracture mechanisms.



## 1. Introduction

Fracture characterization of bone has been attracting the attention of the research community, justified by social and economical impact of skeletal fractures due to ageing, diseases, exercise practicing, occurrence of falls, or pharmaceutical treatments. In this context, fracture mechanics theory emerges as a fundamental tool to deal with bone behavior. Several authors have used concepts of linear elastic fracture mechanics to study the fracture risks of bone under different conditions [1,2]. However, bone is a complex composite material comprised of a mineral phase (hydroxyapatite) and an organic phase (collagen) organized in a hierarchical, heterogeneous and anisotropic microstructure. The consequence is the appearance of a complex fracture behavior with different fracture mechanisms occurring in the vicinity of the crack tip. Hence, non-linear fracture mechanics has become a key tool to deal with such aspects inherent to fracture behavior of bone [3–5]. These studies emphasize the non-negligible fracture process zone that develops ahead of the crack tip, thus making doubtful the application of linear elastic fracture mechanics. Those authors also pointed out the need of proper measurement of the so-called Resistance-curves (*R*-curves), which gives the fracture energy as a function of crack extension [6]. Indeed, the fracture test and specimen geometry must allow full development of fracture process zone, without being perturbed by spurious effects induced, for example, by limited specimen dimensions or boundary conditions. In other words, the fracture test and specimen geometry must provide self-similar crack growth, leading to a plateau on the R-curve that allows a clear measurement

* Corresponding author.
*E-mail address:* mfmoura@fe.up.pt (M.F.S.F. de Moura).

0013-7944/$ - see front matter © 2012 Elsevier Ltd. All rights reserved.
http://dx.doi.org/10.1016/j.engfracmech.2012.10.002

**Nomenclature**

| | |
|---|---|
| $a$ | crack length |
| $a_0$ | initial crack length |
| $a_e$ | equivalent crack length |
| $B$ | specimen width |
| $C$ | specimen compliance |
| $C_0$ | initial specimen compliance |
| $E_L$, $E_T$ | Young's moduli |
| $E_f$ | effective elastic modulus |
| $G_I$ | strain energy release rate |
| $G_{Ic}$ | fracture toughness |
| $G_{LT}$ | shear modulus |
| $2h$ | specimen height |
| $L$ | specimen length |
| $P$ | external applied load |
| $w_b$ | crack opening at the onset of bridging |
| $w_u$ | ultimate relative displacement |
| $\delta$ | applied displacement |
| $\Delta$ | initial crack length correction |
| $\sigma_b$ | strength at the onset of bridging |
| $\sigma_u$ | local strength |
| $\nu_{LT}$ | poisson ratio |

*Acronyms*

| | |
|---|---|
| CBBM | compliance based beam method |
| CL | cohesive law |
| DCB | double cantilever beam |
| FPZ | fracture process zone |
| MECM | modified experimental compliance method |

of the fracture energy. A miniaturized version of the double cantilever beam (DCB) test was proposed in a previous work [5] to determine fracture energy under pure mode I loading, satisfying the above cited requisites.

Ji and Gao [7] proposed the use of the virtual–internal–bond (VIB) model to simulate crack nucleation and growth in a nanoscale composite material with huge differences in strength and stiffness between the constituent phases; in the case of bone, protein (organic) and mineral (inorganic) phases. This fracture model was then used to investigate the failure mechanisms in the nanostructure of biocomposites. A somewhat different but related approach is the cohesive zone modeling (CZM) which is used in macroscale analyses. The CZM establishes a softening relationship between tractions and relative displacements and is used to simulate damage initiation and growth. It has the disadvantage of requiring a pre-existing crack path, but in many cases the crack path is known a priori. In the case of bone, crack tends to propagate along the longitudinal direction, i.e. parallel to the collagen fibers. A relevant issue of this method concerns the shape of the softening part of the cohesive law used to simulate bone fracture. In this context, Yang et al. [4] proposed a bilinear softening law to deal with different failure mechanisms typically observed in bone. The first descending branch of this law intends to describe damage developing just at the crack tip, although the second one depicts the fracture phenomenon in the further crack wake. However, the determination of the cohesive parameters defining the cohesive law was performed by a trial and error manual procedure, consisting on the minimization of the residual difference between the predicted and experimental load–displacement curves. Since bilinear softening laws involve the determination of four independent cohesive parameters (the local strength, the relative displacement and traction corresponding to the inflexion point, and the ultimate relative displacement) the method used by the authors can be viewed as cumbersome.

Another aspect that deserves researchers' attention is the influence of water on the fracture behavior of bone. In bone, water is present in microscopic pores and within extracellular matrix. It has been verified that water decreases with skeletal growth [8] and with its progressive mineralization [9]. Additionally, water distribution, i.e., the amount of water bounded to collagen, to mineral, and the free water in the vascular–lacunar–canalicular cavities, alters during life. For example, Kopp et al. [10] observed that the interaction of water with collagen decreases with age. Consequently, it is obvious that the distribution of water within bone tissue influences its mechanical behavior. As a result of these arguments, the study of the role of water in the mechanical properties of bone is a crucial task, in order to understand the susceptibility of bone to fracture in the elderly population.

In this work, fracture properties of hydrated and dehydrated bovine cortical bone were measured using the DCB test. The main goal is to evaluate the influence of water on bone fracture behavior, i.e., on fracture toughness and on failure modes. Numerically, the respective cohesive laws under pure mode I loading were obtained by means of an inverse method. Two different data reduction schemes were used to determine bone fracture toughness, which is a fundamental input parameter in the determination of the cohesive law. Consistent fracture properties were obtained from both methods which strengthens the validity of the obtained laws. Reliable softening laws for each case (hydrated and dehydrated) were determined, thus allowing trustworthy cohesive parameters adequate for appropriate simulation of bone fracture behavior under mode I loading. Additionally, the different fracture behaviors between the two materials (hydrated and dehydrated) are detailed and thoroughly discussed.

## 2. Experiments

### 2.1. Material characterization

In order to assess the influence of water in the damage mechanism of bone some preliminary material characterization tests were performed. The hydrating process consists on immersing the specimens in physiological saline solution at 37 °C during 24 h till the mass equilibrium is reached. On the other hand, the dehydrating procedure was executed by placing the specimens in a vacuum oven at 37 °C and in presence of a desiccant during 24 h. The objective of the material characterization tests was to determine the mass fractions of the main constituents of bone by means of a thermogravimetric analysis, and the influence of water on the bone hardness through microhardness Vickers tests, and on the material stiffness performing three point bending tests.

### 2.2. Thermogravimetric analysis

In order to check the material variability among the tested specimens and evaluate the effectiveness of hydration and dehydration treatments, thermogravimetric analyses (TG) and Vickers microhardness measurements were performed. The thermogravimetric analyzes (TG) were carried out on a TGA T50 (TA Instruments®) thermobalance, at heating rate of 10 °C/min and under dry nitrogen gas flow. The samples were initially hydrated and its mass was in the range of 15–20 mg. Fig. 1 shows a typical TG curve and its associated derivative thermogravimetric (DTG) curve, i.e., $dm/dT$. The first thermal event, associated with the first peak on the DTG curve, corresponds to water loss. The second thermal event, related with the second peak, corresponds to collagen combustion. The first local minimum of DTG curve (in the range 200–230 °C) was used to estimate the water mass fraction ($\%m_w$), considered equal to the mass loss at that temperature. On the other hand, the final mass fraction (at 700 °C) was assumed to give the mineral mass fraction ($\%m_m$). Hence, the organic mass fraction ($\%m_o$) is the difference to 100%. The results of bone composition ($\%m_w$, $\%m_m$ and $\%m_o$) are summarized in Table 1, revealing a very homogeneous bone sample. The values of $\%m_w$ obtained from TG measurements are in good agreement with the values obtained after the dehydration treatment described above, by simple weighing using a Mettler Toledo electronic balance (resolution of 0.1 mg). This finding demonstrates the efficacy of dehydration treatment.

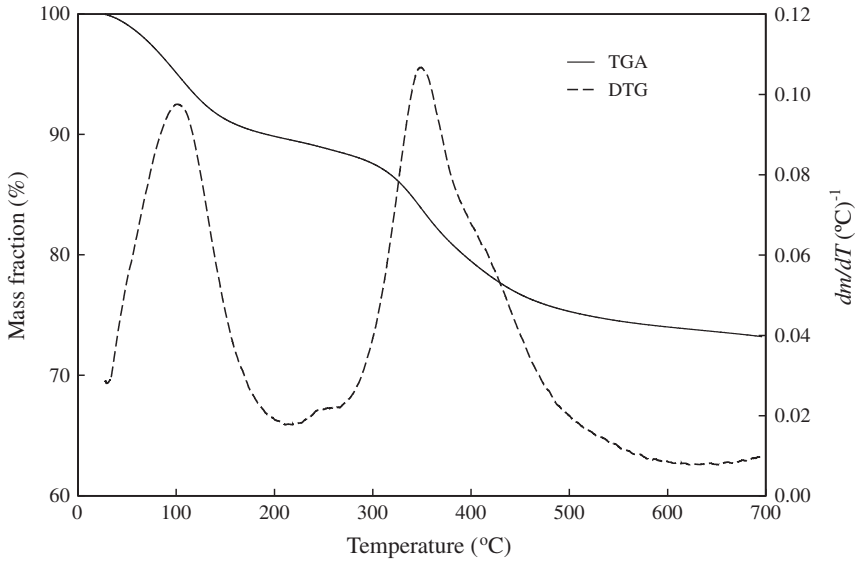


**Fig. 1.** Thermogram (TGA) of cortical bone with its first derivative (DTG).

**Table 1**
Mass fractions obtained by thermogravimetric analysis (three specimens).

| | $\%m_{mineral}$ | $\%m_{organic}$ | $\%m_{water}$ |
|---|---|---|---|
| Average | 70.21 | 18.67 | 11.62 |
| CoV (%) | 0.93 | 2.53 | 2.80 |

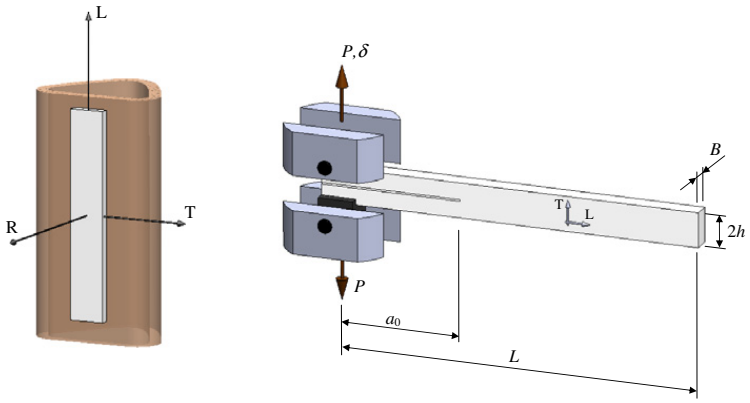


**Fig. 2.** Schematic representation of the DCB test (L: longitudinal direction; R: radial direction, and T: tangential direction of the femur).

### 2.3. Microhardness tests

Microhardness Vickers tests were performed on hydrated and dehydrated bone. Indentations were performed in the RT plane (Fig. 2), i.e., along the osteons direction (direction L) on testing samples. Before microhardness testing, specimens were embedded in a weakly exothermic epoxy (EpoFix, Struers®) and polished to produce the mirror-like surfaces needed for microhardness testing, with silicon carbide abrasive papers of decreasing grit size (220, 500, 800, 1200, 2500 and 4000 grit). The Vickers microhardness measurements were performed using a Shimadzu HMV-2000 tester. To account for local variability of tissue microstructure, five results were collected at randomly chosen locations in each specimen. The results are presented in Table 2. It was observed that dehydrated bone is 73% harder than hydrated one, which emphasizes the importance of water on the material hardness. This remarkable increase of hardness has an effect on the material toughness as discussed in the following sections. Furthermore, this feature reveals that the dehydration treatment removes water not only from the material porosity (vascular canals, lacunae and canaliculi), but also from the extracellular matrix. Indeed, the great increase of Vickers microhardness following the dehydration treatment could be explained from the removal of water from the organic phase of bone.

### 2.4. Elastic modulus

Additionally, the elastic modulus was determined for each specimen since it is a fundamental elastic property which concerns the definition of material stiffness. Being a natural and anisotropic material, bone presents scatter on its elastic properties [11]. In this context, three-point bending tests were executed to measure the flexural modulus $E_L$ in the longitudinal (L) direction considering the beam theory. These tests were performed in the same specimens used for fracture characterization using the DCB test just before the execution of the pre-crack. A servo-electrical testing system (Micro-Tester INSTRON 5848) was used and the maximum displacement of the actuator was within the linear range of material response, thus preventing any damage of specimens.

### 2.5. Specimens preparation

Bone specimens were harvested from fresh bovine femora of young animals (nearly 8 months) within one day post-mortem period. Specimens were cut from the mid-diaphysis following the anatomic orientations illustrated in Fig. 2. A milling

**Table 2**
Hydrated and dehydrated hardness Vickers.

| | Hydrated | Dehydrated |
|---|---|---|
| Average | 47.66 | 82.66 |
| Cov (%) | 4.00 | 3.87 |

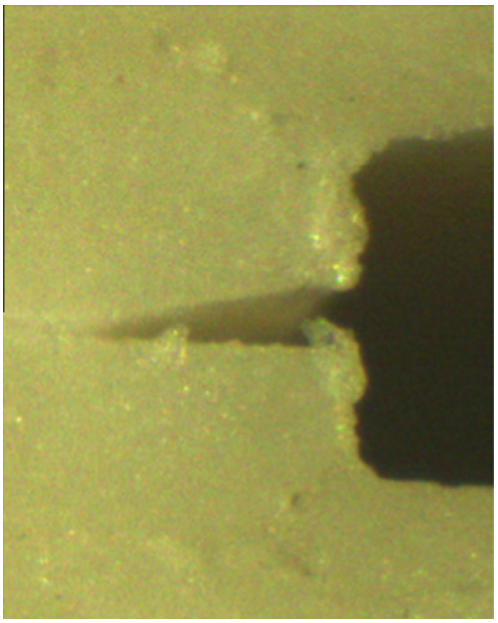

**Fig. 3.** Detail showing the notch and the induced pre-crack.

**Fig. 4.** Photography of the DCB test.

machine was used to remove the endosteal and periosteal tissues. In the course of the machining process, specimens were kept moist using a physiological saline solution. Due to limitation restrictions in bovine femur, the DCB specimens had to be quite small, when compared with other applications using other materials. A total number of twenty specimens were prepared. Half of them were hydrated and the other half dehydrated just before performing flexure and fracture tests.

### *2.6. Double cantilever beam test*

A crucial aspect of the DCB specimens is the execution of the pre-crack, $a_0$. Thus, a two step procedure was followed to guarantee the uniformity of crack fabrication. Hence, an initial notch was introduced using a circular diamond saw with a thickness of 0.3 mm. Subsequently, a small pre-crack was produced (Fig. 3) using a sharp blade mounted in a servo-electrical testing machine (Micro-Tester INSTRON 5848), and displaced 0.15 mm against the notch root at a displacement rate of 100 mm/min.

As illustrated in Fig. 2 specimens were machined in order to allow propagation parallel to osteons direction (i.e., TL propagation system, being T the normal to the crack plane and L the crack propagation direction). The nominal sample dimensions are $L = 60$ mm, $B = 2.7$ mm, $2h = 6$ mm and $a_0 = 18.6$ mm.

Experimental tests (Fig. 4) were performed using a servo-electrical testing system (Micro-Tester INSTRON 5848) under displacement control, imposing an actuator velocity of 0.2 mm/min, in order to induce smooth crack propagation. Load–displacement ($P$–$\delta$) curves were registered with an acquisition rate of 5 Hz.

## 3. Data reduction schemes

Two different data reduction schemes providing Resistance-curves ($R$-curves) were used to evaluate fracture energy of bone under mode I loading. The first one is the modified experimental compliance method (MECM), which requires experimental compliance calibration as a function of the crack length. The second one, named Compliance Based Beam Method (CBBM), is a method based on beam theory and equivalent crack concept.

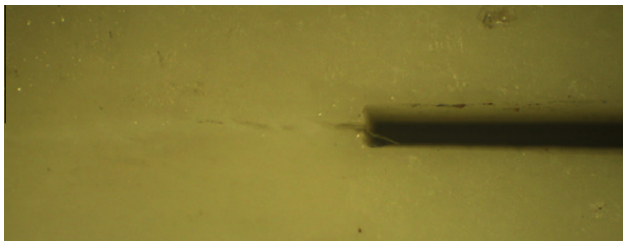

**Fig. 5.** Undefined crack tip in bone under mode I loading.

### 3.1. Modified experimental compliance method

The MECM is based on the following law establishing an empirical relationship between compliance ($C = \delta/P$) and crack length $a$:

$$C = ka^n \tag{1}$$

being $k$ and $n$ constant parameters to be determined experimentally by fitting. Combining Eq. (1) with the Irwin–Kies relation:

$$G_I = \frac{P^2}{2B}\frac{dC}{da} \tag{2}$$

leads to

$$G_I = \frac{nP\delta}{2Ba} \tag{3}$$

This equation requires crack length monitoring during its growth, which is difficult to perform in bone (Fig. 5). This issue constitutes a drawback, since it can lead to incorrect evaluation of fracture energy. To overcome this limitation, experimental compliance calibration considering different initial crack lengths $a_0$ should be carried out. Therefore, from Eq. (1), it can be written:

$$\log_{10} C_0 = n\log_{10} a_0 + \log_{10} k \tag{4}$$

where $n$ and $k$ can be determined through linear regression. The compliance calibration tests were carried out in the same specimens used in the fracture tests, for five initial crack lengths $a_0$ introduced consecutively, and ranging between 19 and 23 mm. Subsequently, during the fracture test, for each point of the $P$–$\delta$ curve an equivalent crack length $a_e$ can be estimated using the previous compliance calibration curve. Therefore, $a_e$ and the actual compliance value $C$ should be considered in Eq. (4) instead of the values used in the calibration procedure ($a_0$ and $C_0$). Finally, the R-curve (i.e., $GI = f(a_e)$) was obtained through Eq. (3), replacing $a$ by $a_e$.

### 3.2. Compliance based beam method

The MECM requires the previous evaluation of the compliance calibration curve, which is a laborious and time consuming task. To overcome this disadvantage an alternative method (known as CBBM [12]) based on specimen compliance, beam theory and crack equivalent concept can be utilized. Hence, considering the Timoshenko beam theory the $C = f(a)$ relationship can be written as [12]:

$$C = \frac{8a^3}{E_L Bh^3} + \frac{12a}{5BhG_{LT}} \tag{5}$$

being $G_{LT}$ the shear modulus in the LT plane (Fig. 2). This equation was obtained assuming a perfect clamping at the crack tip [12], which does not comply with the physical reality. In order to include the effect of root rotation at the crack tip, a correction to the crack length can be incorporated [13],

$$\Delta = h\sqrt{\frac{E_f}{11G_{LT}}\left[3 - 2\left(\frac{\Gamma}{1+\Gamma}\right)^2\right]} \tag{6}$$

where

$$\Gamma = 1.18\frac{\sqrt{E_f E_T}}{G_{LT}} \tag{7}$$

On the other hand, bone is a natural material presenting some variability of its elastic properties, which means that the longitudinal modulus $E_L$ can vary from specimen to specimen. In this context, an effective elastic modulus ($E_f$) can be determined from Eq. (5) considering the initial values of compliance ($C_0$) and crack length ($a_0$) as follows

$$E_f = \left(C_0 - \frac{12(a_0 + |\Delta|)}{5BhG_{LT}}\right)^{-1} \frac{8(a_0 + |\Delta|)^3)}{Bh^3} \tag{8}$$

An iterative procedure involving Eqs. (6)–(8) should be used till a converged value of $E_f$ is reached. During crack growth an equivalent crack length ($a_e$) can be estimated to account for the damaging processes occurring ahead of the crack tip. Effectively, since a non-negligible fracture process zone (FPZ) develops, the energy dissipated in this region should be accounted for, which does not occur if the real crack length is used. In this context, Eq. (5) can be solved to yield $a_e$ as a function of the current compliance in the course of the test ($a_e = f(C)$), using Matlab® software [12].

The R-curve ($G_I = f(a_e)$) can be obtained combining Eqs. (2) and (5), by means of

$$G_i = \frac{6P^2}{B^2h}\left(\frac{2a_e^2}{h^2E_f} + \frac{1}{5G_{LT}}\right) \tag{9}$$

This method presents several advantages. In fact, the crack length monitoring during its growth is not necessary since the equivalent crack is a calculated parameter as a function of the current specimen compliance (data captured from the load–displacement curve). This is a very important aspect, since crack length monitoring in bone fracture is not easy to perform (Fig. 5). In addition, the real crack length does not include the effect of energy dissipation occurring ahead of the crack tip due to the developed non-negligible FPZ. Furthermore, this method accounts for scattering of elastic properties, since the elastic modulus is a computed parameter using the initial values of $a_0$ and $C_0$. From Eq. (9) it can be observed that the shear modulus $G_{LT}$ has a small influence on the results and a typical value can be used.

## 4. Fracture energy

Load–displacement curves obtained during the DCB tests were registered for hydrated and dehydrated bone. Fig. 6 clearly highlights the different curve profiles obtained for each case. Thus, the dehydrated bone presents a higher initial stiffness followed by an abrupt failure, which makes clear its brittle behavior. On the other hand, the hydrated bone shows a more ductile response, illustrated by a pronounced non-linear behavior before the maximum load is attained. Additionally, after the peak-load a soft decrease of load is observed denoting a smooth failure process. This is characteristic of quasi-brittle materials which develop non-negligible fracture process zones ahead of the crack-tip. This can also be observed in the profiles of the respective R-curves plotted in Fig. 7. Effectively, the attainment of a plateau in the hydrated case takes longer than in the dehydrated one (Fig. 7), which emphasizes the role of a larger FPZ development in the former case.

Tables 3 and 4 present the summary of the elastic moduli ($E_L$) and fracture energies for the hydrated and dehydrated bone, respectively. The longitudinal modulus calculated for the dehydrated material is 6.5% higher than the hydrated one. Regarding the fracture energy ($G_{Ic}$) one can affirm that the hydrated bone presents a value more than three times as big as the dehydrated one, thus demonstrating the difference of toughness between these two conditions. This emphasizes the important role of water in the toughness mechanisms of bone. An excellent agreement of the fracture energies at the plateau of the R-curves was obtained using both methods (i.e., MECM and CBBM). This result validates the CBBM, which is much simpler to apply.

It is interesting to note a clear relation between fracture toughness and Vickers microhardness (Fig. 8). As it can be seen, the important increase of hardness with the dehydration process reflects on a remarkable decrease of bone fracture toughness. This is a clear indication that microhardness measurements can be used in systematic studies as an indicator of fracture toughness trends.

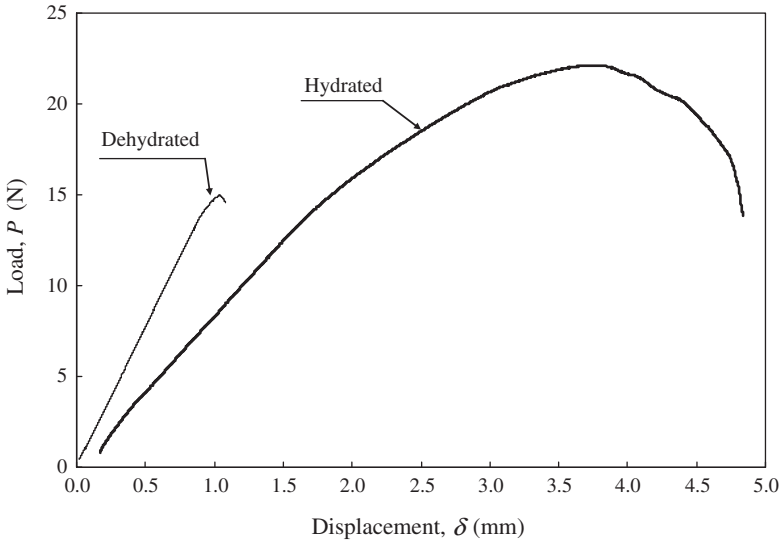


**Fig. 6.** Typical $P$–$\delta$ curves of hydrated and dehydrated young bovine bone.

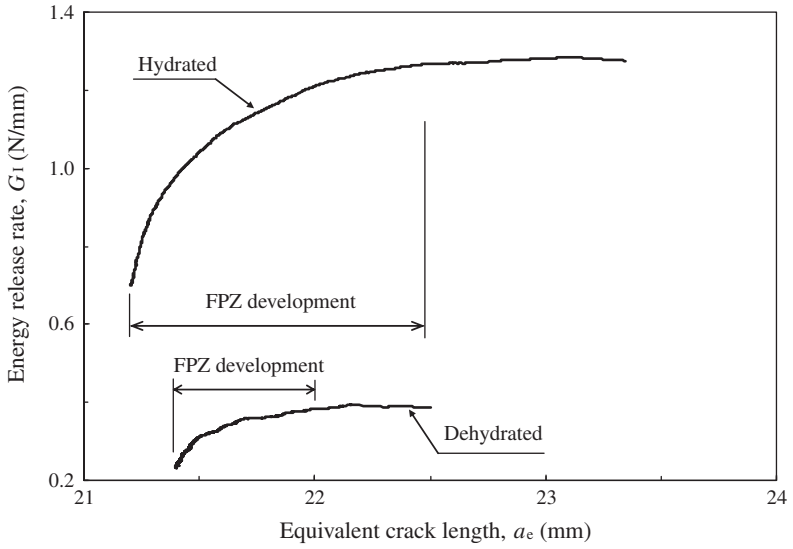


**Fig. 7.** Typical R-curves of hydrated and dehydrated young bovine bone.

**Table 3**
Longitudinal flexure modulus and fracture energy of hydrated bone.

| Specimen | $E_L$ (GPa) | $G_{Ic}$ (N/mm) | |
|---|---|---|---|
| | | MECM | CBBM |
| 1 | 22.07 | 1.67 | 1.80 |
| 2 | 20.46 | 1.25 | 1.26 |
| 3 | 19.07 | 1.96 | 1.97 |
| 4 | 20.22 | 1.56 | 1.49 |
| 5 | 20.75 | 2.65 | 2.59 |
| 6 | 22.08 | 1.82 | 1.84 |
| 7 | 19.69 | 1.95 | 1.93 |
| 8 | 21.08 | 1.55 | 1.68 |
| 9 | 21.56 | 1.44 | 1.47 |
| 10 | 21.84 | 1.73 | 1.68 |
| Average | 20.88 | 1.76 | 1.77 |
| CoV (%) | 5 | 22 | 21 |

**Table 4**
Longitudinal flexure modulus and fracture energy of dehydrated bone.

| Specimen | $E_L$ (GPa) | $G_{Ic}$ (N/mm) | |
|---|---|---|---|
| | | MECM | CBBM |
| 1 | 23.8 | 0.47 | 0.44 |
| 2 | 24.05 | 0.59 | 0.55 |
| 3 | 23.89 | 0.41 | 0.42 |
| 4 | 19.77 | 0.61 | 0.59 |
| 5 | 20.64 | 0.765 | 0.77 |
| 6 | 22.09 | 0.445 | 0.42 |
| 7 | 21.52 | 0.42 | 0.41 |
| 8 | 22.33 | 0.6 | 0.58 |
| 9 | 22.47 | 0.66 | 0.66 |
| 10 | 21.82 | 0.39 | 0.405 |
| Average | 22.24 | 0.52 | 0.54 |
| CoV (%) | 6 | 24 | 24 |

## 5. Cohesive laws

Cohesive laws (CLs) representative of fracture behavior of hydrated and dehydrated bone can be obtained through an optimization strategy involving an inverse method and a genetic algorithm [14]. Fracture energy value determined in the previous section is the fundamental input parameter used in the numerical procedure employed to evaluate the remaining

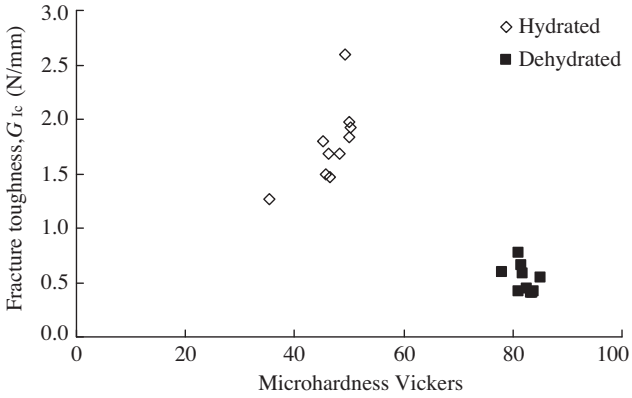


**Fig. 8.** Relation between fracture toughness and Vickers microhardness of bone.

cohesive variables. These variables define the bilinear damage law (Fig. 9) that simulates bone fracture behavior, since the area circumscribed by the CL corresponds to the mode I fracture energy $G_{Ic}$ [12].

Finite element analysis including cohesive zone modeling was used to simulate damage initiation and propagation in the DCB specimens of bone. Fig. 10 illustrates the FE mesh used in the numerical simulations presenting 3840 two-dimensional plane stress solid elements, with 240 interface finite elements positioned in the crack path (i.e., ligament section). Small increments (0.005 of the applied displacement) were used to ensure smooth damage propagation in the course of the loading process, using the elastic properties presented in Tables 3–5.

The difference between the numerical and the experimental load–displacement curves is quantified through an objective function which must be minimized by means of a previously developed genetic algorithm [17]. This optimization procedure interacts with a developed cohesive zone model used to simulate progressive damage and programmed as a user-subroutine

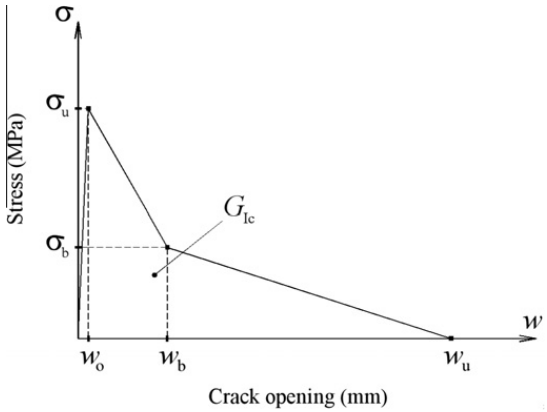


**Fig. 9.** Bilinear cohesive law.

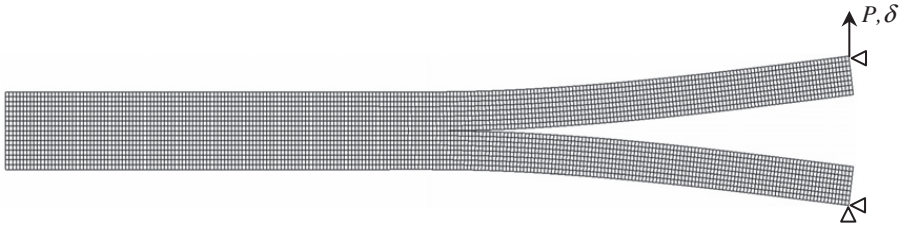


**Fig. 10.** Finite element mesh.

**Table 5**
Nominal mechanical properties of cortical bone [15,16].

| $E_L$ (GPa) | $E_T$ (GPa) | $G_{LT}$ (GPa) | $\nu_{LT}$ | $\sigma_u$ (MPa) |
|---|---|---|---|---|
| –[a] | 9.55 | 4.74 | 0.37 | 20.0 |

[a] Values presented in Tables 3 and 4.

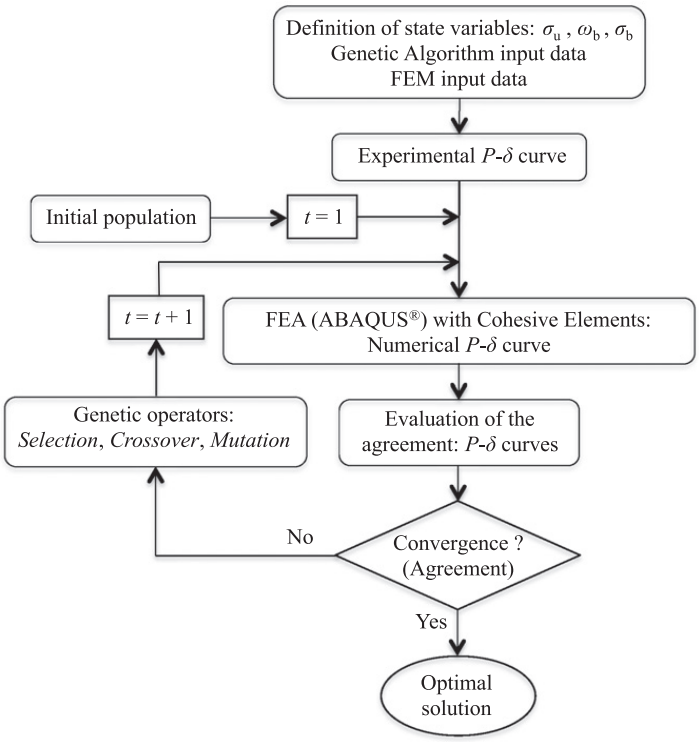


**Fig. 11.** Organogram of the developed genetic algorithm.

of ABAQUS software utilized to perform finite element analysis. As schematically represented in Fig. 11, the identification of the design variables (i.e, $\sigma_u$, $w_b$, $\sigma_b$) defining the bilinear cohesive law (Fig. 9) requires the evaluation of the agreement between the numerical and experimental load–displacement curves. This is made within an evolutionary strategy, which involves the generation of an initial population of potential combinations of design variables and the application of classic genetic operators as Selection, Crossover and Mutation, in successive generations $t$. The optimal combination of design variables is identified once a good agreement between the numerical and experimental load–displacement curves is attained. The agreement between both curves is quantified by means of a defined objective function. As a consequence, the adequate CL is the one which leads to the best agreement between the numerical (given by the evolutionary algorithm) and the experimental load–displacement curve (Fig. 12).

In the optimization procedure a large interval was considered for the local transverse strength ($10 \leqslant \sigma_u \leqslant 90$ MPa) to provide a sufficiently large range to match two studied cases: hydrated and dehydrated bone. Concerning the inflexion point of the bilinear softening law (Fig. 9), the only imposed constraint is that this point ($w_b$, $\sigma_b$) must not go beyond the linear softening law, which is considered as being the limit case. The ultimate relative displacement leading to failure $w_u$ is a function of the fracture energy and is given by:

$$w_u = \frac{2G_{Ic} - \sigma_u w_b}{\sigma_b} \tag{10}$$

Fig. 13 illustrates the cohesive laws obtained for hydrated and dehydrated bone. Several aspects deserve special discussion. Hence, the transverse local strength ($\sigma_u$) of the dehydrated bone is approximately the double of the hydrated one (Fig. 13).

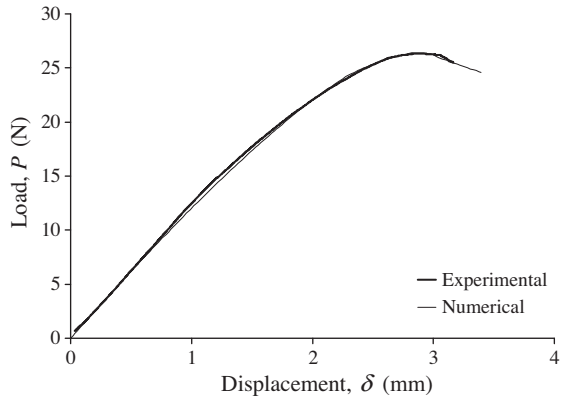


**Fig. 12.** Experimental and numerical load–displacement curves.

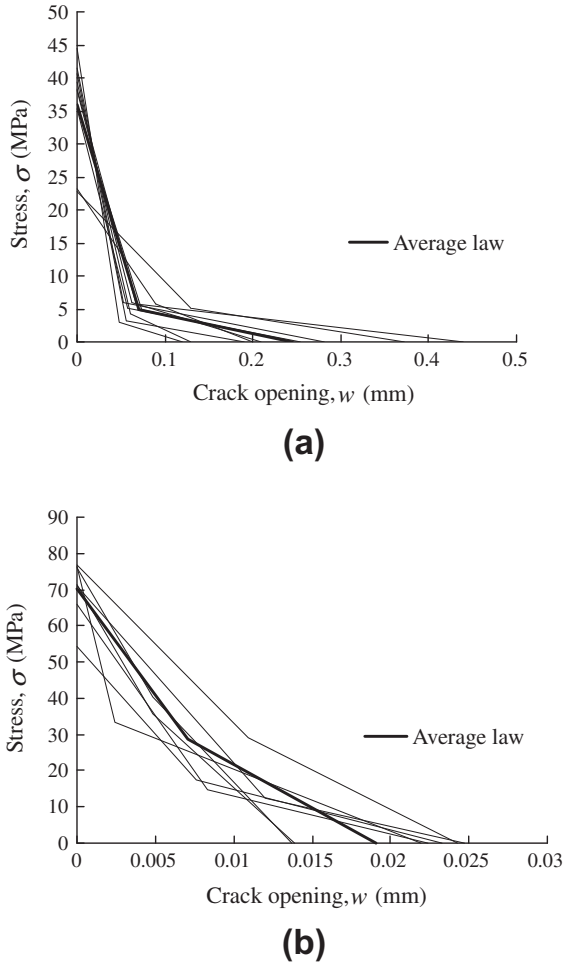


**Fig. 13.** Cohesive laws of the (a) hydrated and (b) dehydrated bone.

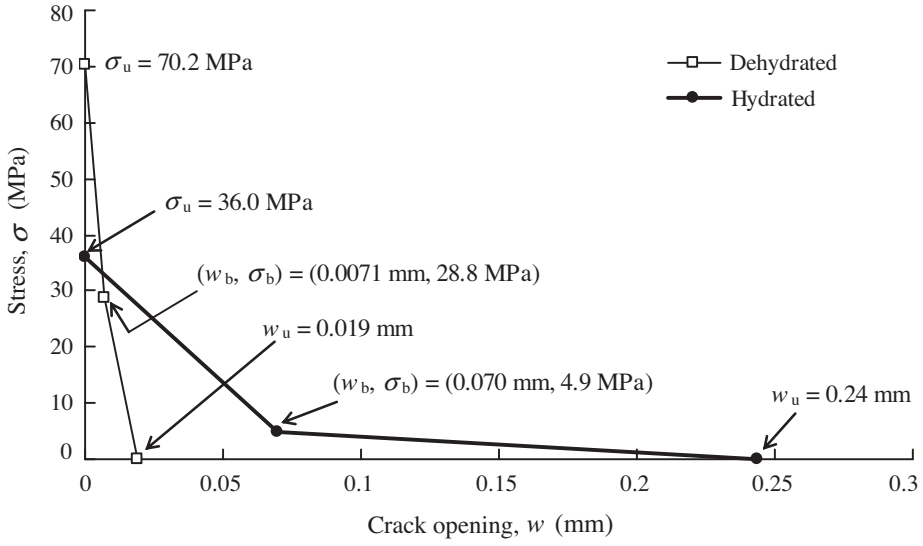


**Fig. 14.** Average cohesive laws for hydrated and dehydrated bone.

Furthermore, the ultimate relative displacement ($w_u$) of the hydrated bone is approximately an order of magnitude higher than the dehydrated case. These two aspects clearly emphasize the different performance of the two analyzed cases, i.e., the hydrated bone is much more ductile than the dehydrated one that clearly denotes a significant brittle behavior. Fig. 14 presents the average cohesive laws for each case. It is clearly shown that different laws are obtained. In fact, the hydrated bone clearly reveals two different branches intrinsically associated to two predominant damage mechanisms. However, the

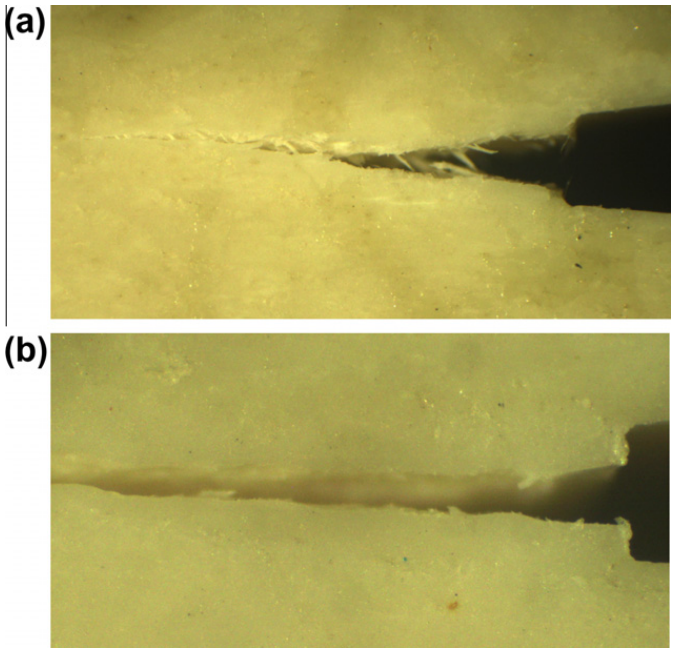


**Fig. 15.** Macroscopic appearance of crack propagation in (a) hydrated and (b) dehydrated bone.

dehydrated bone cohesive law points to a typical linear softening relationship, which means that there is a unique predominant damaging mechanism occurring ahead of the crack tip during the fracture process. These different damage mechanisms can be explained by the collagen influence and its interaction with water. In the hydrated bone, the collagen softens the material, becoming responsible for its more ductile behavior. In fact, according to Yan et al. [18] hydration affects markedly the collagen spacing, thus influencing the hydrogen bonds between collagens. Furthermore, Lees et al. [19] showed that effective molecular diameter of dry collagen is approximately 30% lower than the wet bone collagen. Although during the drying process the mineral phase acts as a constraint, this important reduction adversely affects bone strength and toughness. As a result of this mechanism, different types of failure are observed for wet and dry bone. For the hydrated bone extensive fiber bridging can be observed in the wake of the crack tip (Fig. 15), involving the formation of unbroken regions that span the crack thus resisting to crack opening. Contrarily, the dehydrated bone presents a clear crack without fiber bridging, thus reflecting a more brittle behavior induced by the above described mechanism intrinsic to the drying process.

## 6. Conclusions

Fracture characterization under mode I loading of bovine cortical bone was analyzed in this work using the DCB test. Two independent data reduction schemes applied to the DCB test were utilized to estimate bone toughness. The modified experimental calibration method is based on the achievement of a compliance calibration curve, using different initial crack lengths. Alternatively, the compliance based beam method can be applied to overcome several aspects that are not accounted for in the former method. This last method is based on specimen compliance, beam theory and crack equivalent concept. Its application does not require the elastic modulus measurement for each specimen and crack monitoring during its growth, which is advantageous.

Fracture energy was used as an input parameter to determine the cohesive laws describing fracture behavior of hydrated and dehydrated bone. The referred laws were identified by means of a previously developed inverse procedure involving a genetic algorithm. Two different laws were obtained for each case thus reflecting two distinct fracture behaviors. The dehydrated bone pointed to a linear softening relationship thus showing the existence of one predominant damage mechanism. Contrarily, hydrated bone showed two different branches on the softening law, which are characteristic of two different damage mechanisms occurring during fracture. Effectively, remarkable differences were noted between the hydrated and dehydrated bone in terms of fracture behavior. Wet bone presents a much more ductile behavior which was attributed to the important role of water on the stabilization of the collagen structure thus contributing to increase bone toughness.

It should be emphasized that the proposed procedure can also be used to study the influence of other aspects affecting bone behavior, as is the case of drugs or diseases, for example.

## Acknowledgement

The authors thank the Portuguese Foundation for Science and Technology for supporting the work here presented, through the research Project PTDC/EME/PME/119093/2010.

## References


[1] Norman TL, Vashishtht D, Burr DB. Fracture toughness of human bone under tension. J Biomech 1995;28:309–20.
[2] Wang X, Puram S. The toughness of cortical bone and its relationship with age. Ann Biomed Eng 2004;32:123–35.
[3] Ural A, Vashishth D. Cohesive finite element modeling of age-related toughness loss in human cortical bone. J Biomech 2006;39:2974–82.
[4] Yang QD, Cox Brian N, Nalla Ravi K, Ritchie RO. Fracture length scales in human cortical bone: The necessity of non-linear fracture models. Biomater 2006;27:2095–113.
[5] Morais JJL, de Moura MFSF, Pereira FAM, Xavier J, Dourado N, Dias MIR, et al. The double cantilever beam test applied to mode I fracture characterization of cortical bone tissue. J Mech Behav Biomed 2010;3:446–53.
[6] Koester KJ, Barth HD, Ritchie RO. Effect of aging on the transverse toughness of human cortical bone: evaluation by R-curves. J Mech Behav Biomed 2011;4:1504–13.
[7] Ji B, Gao H. A study of fracture mechanisms in biological nanocomposites via the virtual internal bond model. Mater Sci Eng A 2004;366:96–103.
[8] Jonsson U, Ranta H, Stromberg L. Growth changes of collagen cross-linking, calcium, and water content in bone. Arch Orthop Traum Su 1985;104:89–93.
[9] Robinson RA. Bone tissue: composition and function. Johns Hopkins Med J 1979;145:10–24.
[10] Kopp J, Bonnet M, Renou JP. Effect of collagen cross-linking on collagen-water interactions (a DSC investigation). Matrix 1989;9:443–50.
[11] Rho J-Y, Kuhn-Spearing L, Zioupos P. Mechanical properties and the hierarchical structure of bone. Med Eng Phys 1998;20:92–102.
[12] de Moura MFSF, Morais JJL, Dourado N. A new data reduction scheme for mode I wood fracture characterization using the double cantilever beam test. Eng Fract Mech 2008;75:3852–65.
[13] Hashemi S, Kinloch AJ, Williams JG. The analysis of interlaminar fracture in uniaxial fibre–polymer composites. Proc Roy Soc A – Math Phy 1990;427:173–99.
[14] Tin-Loi F, Que NS. Identification of cohesive crack fracture parameters by evolutionary search. Comput Method Appl M. 2002;191:5741–60.
[15] Dempster WT, Coleman RF. Tensile strength of bone along and across the grain. J Appl Phys 1961;16:355–60.
[16] Dong XN, Guo XE. The dependence of transversely isotropic elasticity of human femoral cortical bone on porosity. J Biomech 2004;37(1281):1287.
[17] Dourado N, Morel S, de Moura MFSF, Valentin G, Morais J. Comparison of fracture properties of two wood species through cohesive crack simulations. Compos Part A-Appl S 2008;39:415–27.
[18] Yan J, Mecholsky JJ, Clifton KB. How tough is bone? application of elastic–plastic fracture mechanics to bone. Bone 2007;40:479–84.
[19] Lees S. A mixed packing model for bone collagen. Calcified Tissue Int 1981;33:591–602.